Extended Advancing Front Technique for the Initial Triangular Mesh Construction on a Single Coil for Radiative Heat Transfer

Zuraida Abal Abas, Shaharuddin Salleh & Zainuddin Manan

Arabian Journal for Science and Engineering

ISSN 1319-8025

Arab J Sci Eng
DOI 10.1007/s13369-013-0556-7

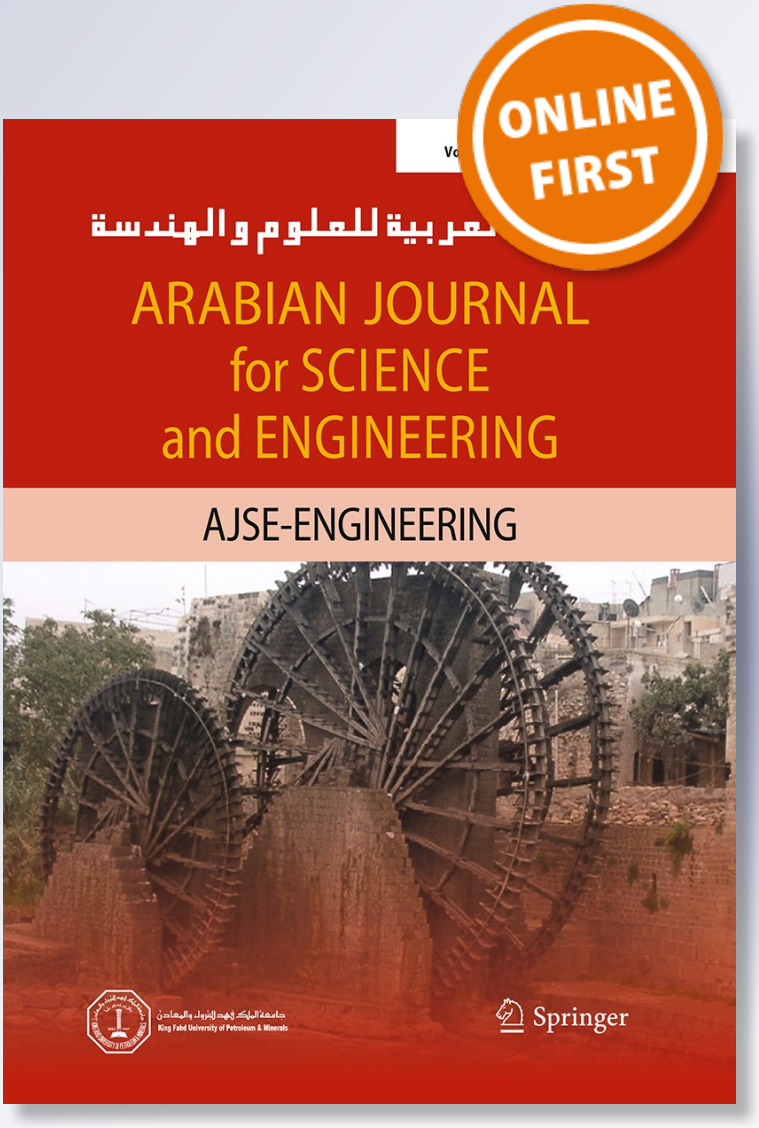

Springer

Arab J Sci Eng
DOI 10.1007/s13369-013-0556-7

RESEARCH ARTICLE - CHEMICAL ENGINEERING

Extended Advancing Front Technique for the Initial Triangular Mesh Construction on a Single Coil for Radiative Heat Transfer

Zuraida Abal Abas · Shaharuddin Salleh · Zainuddin Manan

Received: 10 June 2011 / Accepted: 15 November 2011

Abstract Radiative heat distribution inside an ethylene cracker furnace is often modeled using the finite volume and finite element methods. In both cases, meshes in the form of rectangles and triangles are needed to form the approximating points in the domain. In this paper, a new method called extended advancing Front technique (XAFT) is proposed for meshing the domain inside the cracker furnace, integrated with the deployment of sensors on the wall to obtain the required boundary values. XAFT is the extended version of standard advancing Front technique (SAFT) where the two normal cases in SAFT are extended with six cases of study for the element creation procedure in order to generate the initial mesh. The focus of this method is to construct triangular meshes with the requirements of having the location of sensors deployed along the wall as boundary nodes and to generate nodes at certain boundaries with linearly different lengths. It is also our objective to construct the triangular element iteratively without having to re-order the Front or delete the existing element. There are two contributions from the paper. First is the introduction of six extended cases for the element creation procedure, and second is the layer concept to generate edges with linearly different lengths. XAFT provides the framework for the heat to be approximated using the discrete ordinate method, which is a variant of the finite volume method. Simulation results produced using FLUENT support the findings for effectively approximating the radiation intensity and temperature values inside the furnace.

Keywords Extended advancing Front technique · Discrete ordinate method · Triangular mesh · Radiative heat transfer · Ethylene

الخلاصة

إن نمذجة توزيع الحرارة المُشعّة داخل فرن تكسير الإيثيلين يتم غالبا باستخدام طرق الحجم المحدود والعنصر المحدود. وفي كلتا الحالتين هناك حاجة إلى مشبك على شكل مستطيلات ومثلثات من أجل تكوين النقاط المقربة في المجال. وفي هذه الورقة العلمية تم اقتراح طريقة جديدة سُمّيت بالتقنية الأمامية المتقدمة الممتدة (XAFT) من أجل تناغم المجال داخل فرن التكسر، متحدة مع نشر حساسات على الجدار من أجل الحصول على قيم الحدود المطلوبة.

إن التقنية الأمامية المتقدمة الممتدة هي نسخة ممتدة للتقنية الأمامية المعيارية SAFT ، حيث إن الحالتين الطبيعيتين في التقنية الأمامية المعيارية هما ممتدان مع ست حالات من الدراسة لطريقة إيجاد العنصر من أجل توليد مشبك ابتدائي. إن التركيز في هذه الطريقة هو على إنشاء مشابك مثلثة مع الحاجة إلى وجود موقع للحساسات منتشرة على الحائط كعقد حدود، ومن أجل توليد عقد عند حدود معينة مع أطوال خطية مختلفة. إن من أهدافنا أيضا بناء العنصر الثلاثي تكراريا دون الحاجة إلى إعادة ترتيب الجبهة أو حذف عنصر القائمة. وهناك نوعان من المساهمات في هذه الورقة العلمية ، أولهما تقديم ست حالات موسعة لطريقة إيجاد العنصر، والثاني هو مفهوم الطبقة لتوليد حواف مع أطوال مختلفة خطيا. ويوفر XAFT الإطار للحرارة أن تقرب باستخدام طريقة الإحداثي المنفصل التي هي البديل عن طريقة الحجم المحدود. وتدعم نتائج المحاكاة الناتجة باستخدام FLUENT نتائج التقريب الفعال لكثافة الإشعاع وقيم درجة الحرارة داخل الفرن.

Z. Abal Abas (✉)
Faculty of Information and Communication Technologies, Universiti Teknikal Malaysia Melaka, 76100 Durian Tunggal, Melaka, Malaysia
e-mail: zuraidaa@utem.edu.my

S. Salleh
Mathematical Sciences Department, Faculty of Science, Universiti Teknologi Malaysia, 81310 Johor Bahru, Malaysia
e-mail: ss@utm.my

Z. Manan
Faculty of Chemical Engineering, Universiti Teknologi Malaysia, 81310 Johor Bahru, Malaysia
e-mail: zain@cheme.utm.my

Published online: 06 February 2013

1 Introduction

Ethylene is an important chemical compound produced in the petrochemical industry which is produced from the steam cracking process in ethylene cracker furnaces [1]. In steam cracking, heat is used for breaking or cracking down the saturated hydrocarbon or feedstocks into smaller hydrocarbon in the coils or reactor tubes, which eventually produces the desired products such as ethylene.

Radiation is a heat transfer process which plays a significant role in ethylene production. It has been noted in [2] that 90 % of the heat transfers in the furnace involve radiation. Radiation is caused by energy emission in the form of electromagnetic waves or streams of photons [3]. The burners which are located on the floor near the furnace wall heat up the furnace. This happens because the combustion process carried out in the burner resulted in flames and the release of its hot flue gas. The radiative heat from the furnace wall and hot flue gas is transferred to reactor tubes/coils.

Structured or unstructured triangular mesh formation is an important step in approximating solutions to boundary value problems. One such method is the advancing Front technique where its key algorithmic step is the creation of new elements in the empty region [4]. The method creates a new element by considering *ideal points* which are generated along with the existing nodes in the circle. The ideal point in this case is the centre of the circle, while the radius is calculated based on the empirical rules from the element creation procedure. The advancing Front technique is guaranteed to preserve the boundary integrity as well as having the capacity to create triangular elements with high aspect ratios in the boundary-layer region [5].

In [4], the triangulation process of a closed two-dimensional region was proposed. The method involves steps for generating the elements and reading their boundary values, smoothing the grids and labeling the nodes. The method focuses on nodes renumbering to make way for the Cuthill–McKee algorithm [6] in estimating the matrix bandwidth [7], to be applied for producing smaller bandwidths in order to reduce the storage and amount of computation time.

Sazonov et al. [8] proposed a model which generates near-boundary elements with their own modified form of advancing Front techniques to allow a new node to be located based on the length of the adjacent edges in its Front and the angle between the edges. The points for insertion in this model are determined based on a repeated procedure according to the angle between the edges and the range from a number of nodes. The model also stitches together two different meshes to provide a consistent mesh for the whole domain.

Ito et al. [9] proposed a robust and low computational approach for a parallel framework to generate large-scale meshes for partitioning a coarse tetrahedral mesh into a number of sub-domains using a partitioning algorithm called METIS. The model is based on the parallel advancing Front method to generate the volume mesh in each sub-domain.

In [10], the author highlighted three cases as being possible during the element-creation procedure:

1. A new element is created with a new node as a vertex in which the new node is joined to the edge being considered.
2. An already existing Front node satisfying certain conditions in the proximity of the edge being considered is used to create a new element.
3. Neither of the cases above in which an efficient algorithm of mesh generation should be able to tackle such a problem.

In the present paper, a new algorithm called the extended advancing Front technique 2 (XAFT) is proposed. The algorithm is based on a single coil for producing the initial unstructured grids based on six different cases. These six cases are the extensions from the normal cases in [5,10] and they are able to solve the problems highlighted in [10] specifically on the third case highlighted above. The technique takes into account the deployment of sensor nodes as boundary nodes which supply input values into the system. The technique makes use of the layer concept. Radiative heat transfer in the ethylene cracker furnace can be modeled using the discrete ordinate method by transforming the radiative heat equations into a set of simultaneous partial differential equations based on a discrete representation of the directional variation of the radiation intensity [3].

2 Problem Statement

The problem can be stated as follows. Given a set of sensors distributed along the wall of an ethylene furnace, in what way can the sensors be deployed to provide input in the form of boundary values to approximate the temperature of the flue gas and the incident radiation inside the furnace?

In this problem, the approximation based on the two-dimensional cross-section of the furnace involving cases with an arbitrary number of coils is discussed. Figure 1a shows the horizontal cross-section of a furnace with a set of four coils. Approximation to the boundary value problem involves three processes, namely, structured or unstructured grid generation, physical process model development and discretization using finite difference, finite volume or finite elements. In some specific problem, the process of generating the grid is identified to be affected if sensors are deployed. The values provided by the sensors are crucial as they form the boundaries in the domain. Therefore, their locations in the domain determine the overall shape of the triangular mesh which, in turn, affects the radiation intensity and temperature approximations.

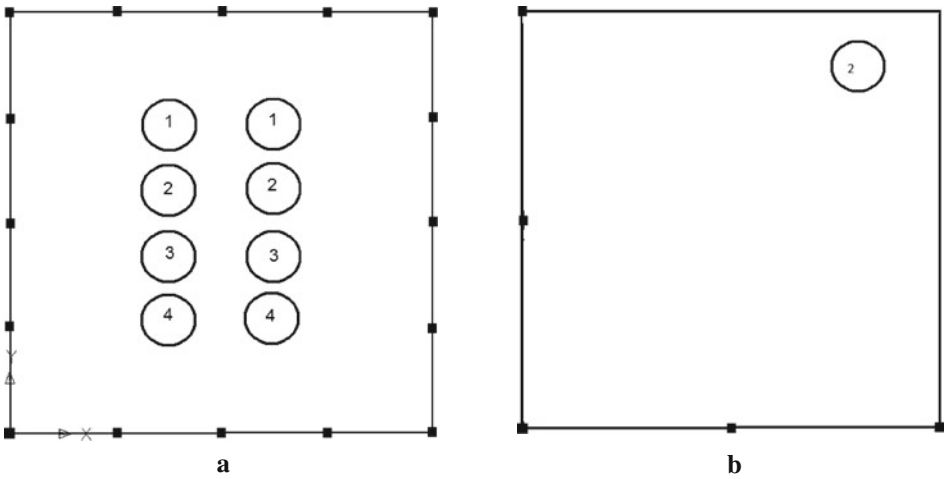

Fig. 1 **a** Top view of the furnace. **b** A simplified problem domain for the initial study

The focus of the present paper is to improve the unstructured grids by modifying the existing standard method in order to produce a mesh which satisfies the requirement of having the sensor placed at the boundary as the nodes for the boundary elements. The sensors are assumed to be placed as illustrated in Fig. 1a. In the original problem, there are four reactor coils in one furnace. Each coil has an inlet and an outlet. Therefore, the cross-sectional view of the furnace gives two circles for every coil.

In this study, we assume only two coils (four circles) are placed at the centre of the furnace. As an initial study, the whole domain of the simplified furnace is divided into four regions. At present, only half of the coil or one quarter at the bottom left corner of the whole domain is considered (as illustrated in Fig. 1b) in order to show how the new enhanced algorithm works. Therefore, this study only considers the initial mesh formation on a single coil.

3 SAFT and the Numerical Method

3.1 Basic Steps of SAFT

Advancing Front technique is a type of unstructured triangulation grid generation method which preserves the boundary integrity as well as having the capacity to create the clustering high aspect-ratio triangles in boundary-layer regions [5]. The boundary curves are discretized by dividing the boundary curves into straight line segments or edges where the nodes are placed on each of the segments or edges. Here, (a, b) denotes the edge formed by nodes a and b. Figure 2a shows a simple two-dimensional domain with connected boundary curves while Fig. 2b shows the discrete elements of the boundary denoted by $(1, 2), (2, 3), (3, 4), \ldots, (10, 1)$.

Front is defined as a set of active edges that are actively available for element triangulation. Referring to Fig. 2b, edges $(1, 2), (2, 3), (3, 4), \ldots, (10, 1)$ form the first or initial Front. The Front is updated continuously when the triangular element is created. This can be seen in Fig. 3, which refers to [11]. It must be noted that all the edges belonging to the current Front are called *active edges* while the edges that are deleted from the current Front list are called *passive edges*. The nodes which compose the active edges in the current position of the Front list are called *active nodes*.

The main idea in controlling the grid in terms of size and shape of the triangular element is the definition of the required grid-cell characteristic through the background grid generation [4,5,10,12–15]. The grid-cell characteristics, known as grid cell parameters, are the size parameter δ, the stretching s and the orientation of the cells φ [5]. For example, Fig. 2b illustrates the background grid consisting of two triangles ABC and ADC. The grid cell parameters are required to be specified at each node for forming the background grid, where in this example are nodes A, B, C and D. In the creation of the triangular element, once the edge is selected from the Front for triangulation, the position of the ideal point (IP) [5] on the perpendicular bisector of the edge is computed in such a way that an equilateral triangle is formed with IP as the third vertex.

Figure 4a illustrates how the edge (a, b) is selected to correspond to the position of IP. In SAFT, the grid cell

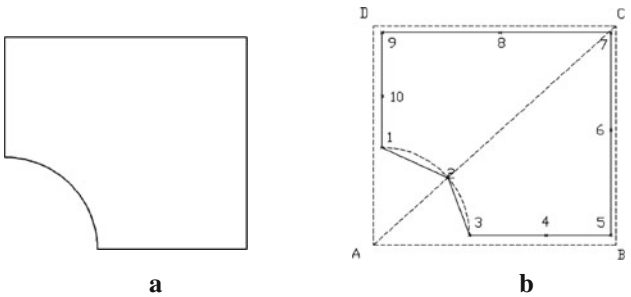

Fig. 2 **a** A two-dimensional domain with connected boundary curves. **b** A set of edges forming the initial Front and the background grid which are formed from *triangles ABC* and *ADC*

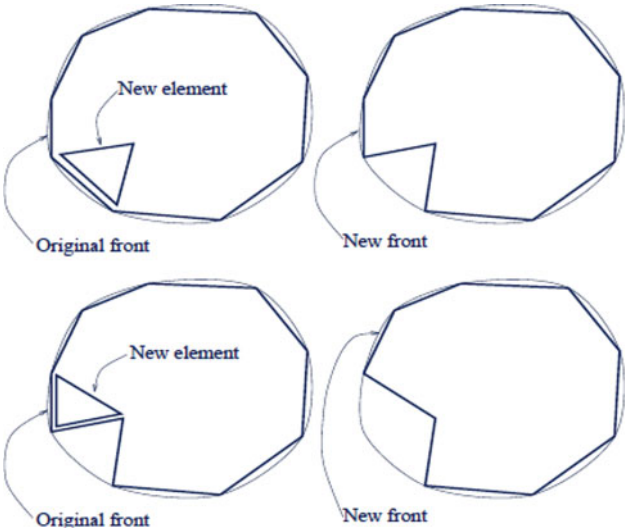

Fig. 3 The illustration of element with regards to Front, taken from [11]

parameters for all nodes in the Front are interpolated in such a way that the edge with the shortest length l in the Front is selected as a departure zone in order to create the triangular element. In order to obtain δ for the next step of calculation, the interpolated values of δ corresponding to the two nodes of the edge are averaging. A circle with centre at IP is constructed with the following empirical formula for the radius, $r = 0.8 \times \delta'$, where [5]

$$\delta' = \begin{cases} 0.55 \times l; & \delta < 0.55 \times l \\ \delta; & 0.55 \times l \leq \delta \leq 2.0 \times l \\ 2.0 \times l; & \delta > 2.0 \times l \end{cases} \quad (1)$$

Figure 4b illustrates a circle with its centre at IP and the radius of the circle following the empirical rule. Active nodes that lie within the circle are searched (if any) and their distances from IP are listed. The best candidate for the third vertex of the triangular element would be the closest one to the IP. The equilateral triangle is constructed if there are no such active nodes lying within the circle. However, the validity of the IP becoming the node must be checked by which it needs to satisfy the following conditions [5]:

1. The coordinate of IP does not lie inside another existing triangular element.

Fig. 4 **a** The selected edge (a, b) and the position of IP. **b** *A circle* is constructed with centre at IP and the radius of the circle following the empirical rule

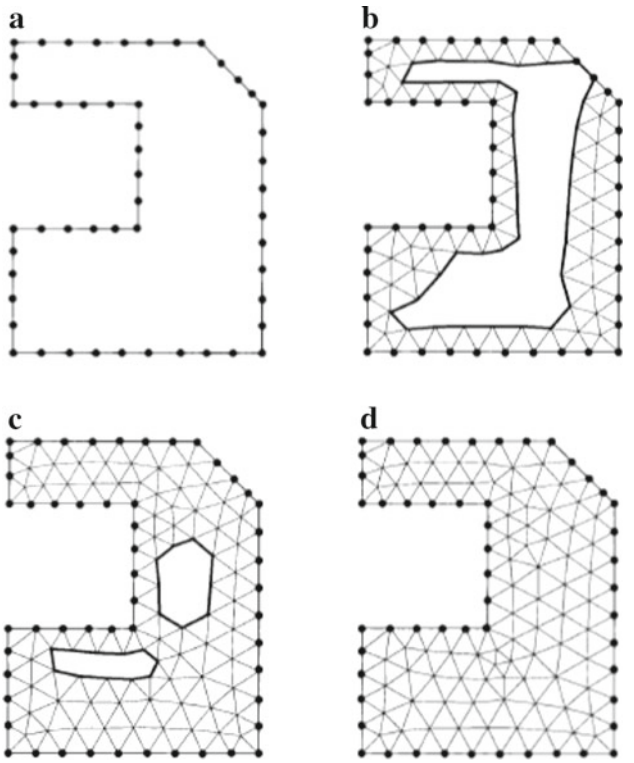

Fig. 5 The illustration of the Front 'marching' process into the interior of the domain, taken from [16]

2. There is no intersection between the side of the new triangular element and any existing sides of the active Front.

Generally, the Front progressed into the interior of the domain in a 'marching' [5,16] process as a result of producing a triangular element in which new nodes and edges are created and at the same time old related edges are deleted, as illustrated in Fig. 5. The new triangular element is constructed by two nodes of a segment of a Front and another node, either a newly created one or one that has already existed in the Front. This process is continued until there are no longer any active edges in the Front list. The general scheme of SAFT is illustrated as in Fig. 6.

3.2 The Concept of Radiation

A high rate radiation is emitted by materials at high temperatures. The emissive power E is the rate of heat flow per unit surface area emitted by a radiating surface. For a black body, the emissive power E_b is given by [17]

$$E_b = \sigma T^4 \quad (2)$$

In Eq. (2), $\sigma = 5.67 \times 10^{-8}$ is Stefan–Boltzmann's constant and T is absolute temperature. The intensity I is the rate of heat flow received per unit area perpendicular to the

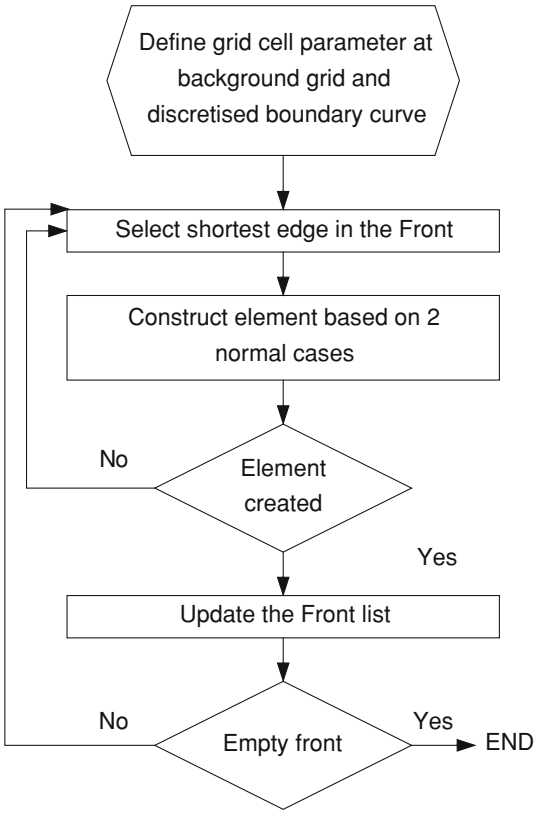

Fig. 6 The general scheme of SAFT

rays and per unit solid angle. The intensity of the black body I_b is [17]

$$I_b = E_b/\pi = \sigma T^4/\pi \tag{3}$$

Equation (3) is used to compute the emitted intensity from the surfaces and fluids. However, for a real surface or gray surface, the emissive power, E_s with surface emissivity ε is given by [17]

$$E_s = \varepsilon\sigma T^4 \tag{4}$$

The emitted intensity I_s is the product of its surface emissivity and the black body intensity [17]

$$I_s = \varepsilon I_b = \varepsilon\sigma T_s^4/\pi. \tag{5}$$

When combustion occurs, large amounts of carbon dioxide and water vapor are produced. These combustion products are both strong absorbers/emitters in the infrared part of the spectrum and the fluid is called a *participating medium* [17,18]. The interaction between the participating fluid medium and radiation can be measured in terms of the absorption coefficient, κ, and its scattering coefficient, σ_s. The sum of these two properties is called the *extinction coefficient* β which is given by $\beta = \kappa + \sigma_s$ [17].

The general relationship that governs the changes in radiation intensity at a point along the radiation ray due to emission, absorption and scattering in a fluid medium is given as [3,17]

$$\frac{dI(\mathbf{r},\mathbf{s})}{ds} = \kappa I_b(r) - \kappa I(r,s) - \sigma_s I(r,s) + \frac{\sigma_s}{4\pi}\int_{4\pi} I_-(s_i)\Phi(s_{,s})d\Omega_i \tag{6}$$

In the above equation, $I(\mathbf{r},\mathbf{s})$ is the intensity of radiation at a location indicated by position vector $\mathbf{r}$ in direction $\mathbf{s}$ and $I_-(s_i)$ is the incident intensity from all possible directions s_i. $\Phi(s_i, s)$ is the scattering phase function which describes the probability of a ray from one direction s_i being scattered into a certain direction s while $\mathbf{d\Omega_i}$ is a solid angle [3]. The first, second, third and fourth terms in the right-hand side equation are the emitted intensity, absorbed intensity, out-scattered intensity and in-scattered intensity, respectively. Equation (6) is integrated over each triangular element in the mesh and it is subject to the boundary conditions, as follows [17]:

$$I(r_w, s) = \varepsilon I_b(r_w) + \frac{(1-\varepsilon)}{2\pi}\int_{2\pi} I_-(r_w, s_i)n.s_i d\Omega_i \tag{7}$$

In Eq. (7), r_w is the position vector of a point on a diffusively emitting and reflecting opaque surface and n is the outward surface normal.

3.3 Discrete Ordinate Method (DOM) and its Integration with the Mesh

Using DOM, Eqs. (6) and (7) are solved for a set of n various directions s_i, $i = 1, 2, \ldots, n$. A numerical quadrature replaces the integral over direction as follows [3,17]

$$\int_{4\pi} f(\mathbf{s})d\Omega \cong \sum_i^n w_i f(s_i). \tag{8}$$

In Eq. (8), w_i is the quadrature weight associated with direction s_i [3]. Therefore, the approximation of Eq. (6) is achieved through a set of n equations, as follows [3,17] :

$$\frac{dI(\mathbf{r},\mathbf{s}_i)}{ds} = \kappa I_b(\mathbf{r}) - \beta I(\mathbf{r},\mathbf{s}_i) + \frac{\sigma_s}{4\pi}\sum_{j=1}^n w_j I_-(\mathbf{s}_j)\Phi(\mathbf{s}_i,\mathbf{s}_j), \tag{9}$$

where $i = 1, 2, \ldots, n$ is subject to the boundary conditions given by [17]

$$I(\mathbf{r}_w,\mathbf{s}_i) = \varepsilon(\mathbf{r}_w)I_b(\mathbf{r}_w) + \frac{1-\varepsilon(\mathbf{r}_w)}{\pi}\sum_{j=1}^n w_j I_-(\mathbf{r}_w,\mathbf{s}_j)\left|\mathbf{n}.\mathbf{s}_j\right|. \tag{10}$$

The angular ordinates $s_j = \xi i + \eta j + \mu k$ and the angular weights w_j are available in [3] where this angular

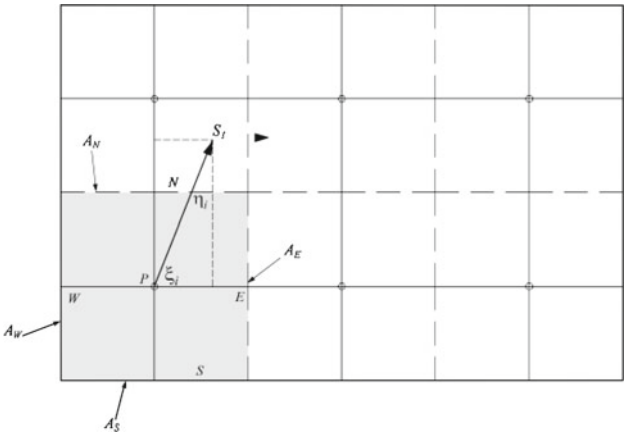

Fig. 7 A general two dimensional geometry to illustrate the DOM, taken from [17]

approximation will transform the Eq. (9) into a set of coupled differential equations in which for Cartesian co-ordinates it would be as follows [17]

$$\xi_i \frac{\mathrm{d}I_i}{\mathrm{d}x} + \eta_i \frac{\mathrm{d}I_i}{\mathrm{d}y} + \mu_i \frac{\mathrm{d}I_i}{\mathrm{d}z} + \beta I_i = \beta S_i \quad i = 1, 2, \ldots, n \tag{11}$$

In Eq. 11, ξ_i, η_i and μ_i are the direction cosines of direction i and

$$S_i = (1-\omega) I_\mathrm{b} + \frac{\omega}{4\pi} \sum_{j=1}^{n} w_j I_j \Phi_{ij} \quad i = 1, 2, \ldots, n \tag{12}$$

In the above equation, $\omega = \frac{\sigma_s}{\beta}$ is the single scattering albedo [17].

Equation (11) is integrated over the control volume by applying the finite volume approximation, by using the area shown in the two dimensional control volume as illustrated in Fig. 7 taken from [17], the following equation are obtained [3,17]

$$\begin{aligned} &\xi_i (I_{E_i} A_E - I_{W_i} A_W) + \eta_i (I_{N_i} A_N - I_{S_i} A_S) \\ &= -\beta I_{P_i} (\Delta V) + \beta S_{P_i} (\Delta V) \quad i = 1, 2, \ldots, n \end{aligned} \tag{13}$$

In Eq. (13), A_W and A_E are the face area in the x-direction while A_S and A_N are the face area in the y-direction where $A_W = A_E = \Delta y$, $A_S = A_N = \Delta x$ and $\Delta V = \Delta x \Delta y$ [3]. I_{P_i} and S_{P_i} are both volume averages of the intensity and the source functions. The approximation of the intensity I_{P_i} which is at the centre of the cell is [3,17]

$$I_{P_i} = \gamma I_{E_i} + (1-\gamma) I_{W_i} \tag{14}$$

$$I_{P_i} = \gamma I_{N_i} + (1-\gamma) I_{S_i} \tag{15}$$

In order to relate the cell edge intensities to the volume average intensity, a weighting factor, γ is used where the most frequent values of γ are set to be 0.5 for the diamond scheme and 1.0 for the step scheme, respectively [17,19]. Referring to Fig. 7, I_{W_i} and I_{S_i} are known for this particular cell since it is a boundary value, therefore, Eqs. (14) and (15) would be as follows [17]

$$\gamma I_{E_i} = I_{P_i} - (1-\gamma) I_{W_i} \tag{16}$$

$$\gamma I_{N_i} = I_{P_i} - (1-\gamma) I_{S_i} \tag{17}$$

Equations (15) and (16) are substituted in Eq. (12) and rearranging gives [17]

$$I_{P_i} = \frac{\beta(\Delta V)\gamma S_{P_i} + \xi_i A_{WE} I_{W_i} + \eta_i A_{SN} I_{S_i}}{\beta(\Delta V)\gamma + \xi_i A_E + \eta_i A_N} \tag{18}$$

where

$$A_{WE} = \gamma A_W + (1-\gamma) A_E \tag{19}$$

$$A_{SN} = \gamma A_S + (1-\gamma) A_N \tag{20}$$

I_{E_i} and I_{N_i} can be obtained once I_{P_i} is calculated and the same process is repeated in the next cell by having the newly calculated values as boundary values for the next cell. This goes on until all the cells are covered and are following the entire ordinate direction.

The temperature value at the boundary faces is used to calculate the blackbody intensity as in Eq. (3). The value of the blackbody intensity is then substituted in the boundary condition in Eqs. (7) and (10) since the boundary face is a part of the surface enclosure. The calculation is done element by element until all directions have been covered and the convergence criteria are met.

4 The Algorithm of Extended Advancing Front Technique-1 (XAFT)

The contribution of this paper is a new algorithm called the *Extended Advancing Front Technique-2* for one-circle for the triangular mesh generation (XAFT). XAFT is an improvement to the SAFT for the initial unstructured triangulation grid generation. The algorithm of XAFT is applicable to the domain with one inner boundary. It still uses the concept of the SAFT where the Front moves into the interior of the domain in a 'marching' process. It must be noted that the terms edge, Front, active edge, passive edge, active node, ideal point (IP) in XAFT are similar to those explained in SAFT in Sect. 3.1.

The endpoints of outer boundary curves in the domain make the first set of nodes created in order to prepare for the triangular mesh generation, as illustrated in Fig. 8a. This is followed by all the nodes created at the boundary curves resulting from discretized boundary curves (both inner and outer boundary) into boundary edges, as illustrated in Fig. 8b. It must be noted that in the XAFT algorithm, nodes are placed at the location of sensor deployments where a boundary edge is formed automatically between two sensors. For outer boundary curves without sensors as in our case, the layer

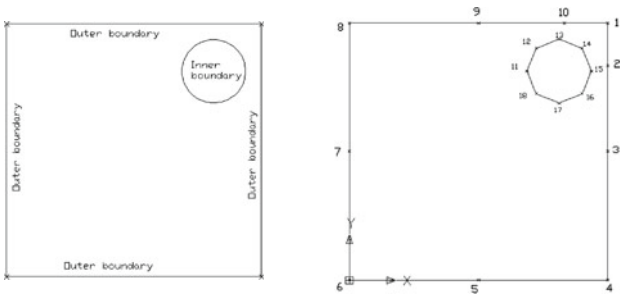

Fig. 8 **a** Foundation of endpoints of all boundary curves. **b** Nodes at outer and inner boundary curves. Nodes 4, 5, 6, 7 and 8 represent the sensors. Nodes 1, 2, 3, 9 and 10 resulting from the layer concept

concept is applied to generate edges with varying length linearly when placing the nodes. The layer concept is referred to in Sect. 4.1.

In general, XAFT considers the inner boundary edges in element construction first until all the inner boundary edges become passive edges. The element construction is then followed by all the active edges in the Front. Hence, the initial Front list is arranged by firstly composing all the inner boundary edges, followed by the outer boundary edges, since the priority is given to inner boundary edges. For example, based on Fig. 8b, the initial Front is:

Initial Front:

(11, 12)(12, 13)(13, 14)(14, 15)(15, 16)(16, 17)(17, 18)
(18, 11)(1, 2)(2, 3)(3, 4)(4, 5)(5, 6)
(6, 7)(7, 8)(8, 9)(9, 10)(10, 1)

The active edge with the shortest length in the Front is selected as the departure zone for triangular element construction. In XAFT, the current selected active edge considered for triangular element construction is called the base edge. For example, referring to Fig. 9a, of all the active edges in the Front, (11, 12) are currently selected for triangular element construction; therefore, (11, 12) is called a base edge. Once the base edge is identified, the position of IP on the perpendicular bisector of the base edge is computed in such a way that an equilateral triangle is formed with IP as the third vertex. The easiest way to compute the IP satisfying the above condition is to form a circle (with radius equal to the length of the base edge and centre at the node, respectively) at each node of the base edge as illustrated in Fig. 9a. Basically, there are two intersection points at first, but the one that lies inside the Front or inside acceptance region is chosen. The chosen intersection point of these two circles is the IP. The two circles constructed previously are deleted in order to avoid confusion while the IP remains in the domain as illustrated in Fig. 9b.

A circle with its centre at IP is constructed with a radius equal to the length of base edge as illustrated in Fig. 9c. IP

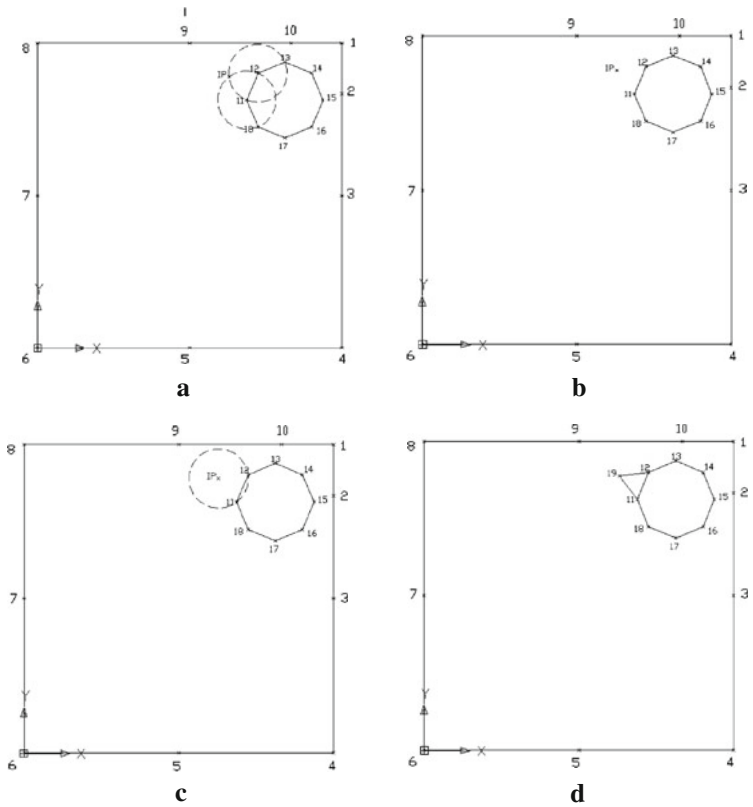

Fig. 9 **a** The base edge is (11, 12). *Intersection point of the two circles* is the IP. **b** IP on the perpendicular bisector of the base edge. **c** A *circle* is constructed with IP as centre. **d** A *triangular element* is constructed by having IP as the node

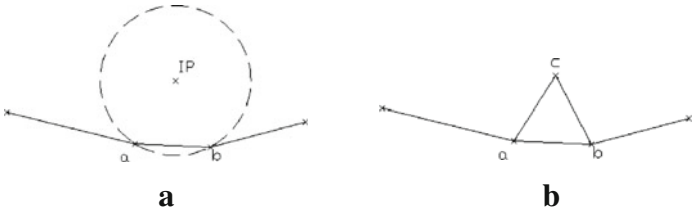

Fig. 10 **a** No object lies within the *circle*. **b** An *equilateral triangle* is constructed

becomes the new vertex of the equilateral triangle constructed since there are no active nodes lying within the circle and two newly created active edges are formed automatically as illustrated in Fig. 9d. It must be noted that once the triangular element is constructed, the Front needs to be updated in which the base edge becomes a passive edge and is deleted from the Front list. At the same time, the newly created active edges are added to the Front list. With Fig. 9d as an example, the new updated Front is as follows where (11, 12) is deleted and newly created edges which are (11, 19) and (19, 12) are added to the list.

The second Front:

(11, 19)(19, 12)(12, 13)(13, 14)(14, 15)(15, 16)(16, 17)
(17, 18)(18, 11)(1, 2)(2, 3)(3, 4)(4, 5)
(5, 6)(6, 7)(7, 8)(8, 9)(9, 10)(10, 1)

The same procedure is repeated to construct the next triangular element, in which base edge is selected; IP is constructed and a circle with radius equal to the length of the base edge and its centre at IP is constructed. A construction of triangular elements using the algorithm of XAFT is actually based on the condition of objects lying within the circle or at the circum circle. The term 'objects' in XAFT refers to any active nodes or active edges. This is where the construction of the triangular element is based on six cases of consideration during the element creation procedure according to the XAFT algorithm.

Case 1 The first case (Case 1) is the simplest one in which the current base edge considered is (a, b) as in Fig. 10a. A circle at centre IP with radius equal to the length of the base edge is constructed. IP becomes the third vertex of the triangular element if there is no object lying within the circle in which it automatically changed to node c as in Fig. 10b. The newly created active edges(a, c) and (b, c) become the sides for the triangular element. The element constructed is an equilateral triangle since all three sides or edges have equal length as illustrated in Fig. 10b.

Case 2 The current base edge considered is (a, b) as illustrated in Fig. 11a for Case 2. A circle at center IP with a radius equal to the length of base edge is constructed. There are two types of objects lying within the circle. The first one is the two nodes which are d and e. The second type of object comprises three active edges intersected with the circle which are (b, c), (c, d) and (d, e). Priority is given to nodes when it comes to selection if both objects occur simultaneously within the circle. If there are multiple active nodes in the circle, calculate all the distance of every active node from the IP. The active node which is the closest one to the IP is selected as the third vertex for triangular element. As illustrated in Fig. 11b, node d is selected as the vertex; therefore, a triangular element is constructed with (a, b), (a, d) and (b, d) as the three sides.

Case 3 At the same time, there is another triangular element being constructed automatically since the three edges are connected to themselves. This condition belongs to Case 3 in XAFT. As illustrated in Fig. 11b, a triangular element is constructed automatically when (b, d) is formed. The three edges (b, c), (c, d) and (b, d) are connected to themselves, and they become the sides of the second triangular element.

Case 4 Figure 12a, b shows the construction of triangulation element following the fourth case (Case 4). Let us say the base edge considered is (a, b), where a circle with radius equal to the length of the base edge and at centre IP is constructed. Based on the figure, it can be seen that the only object involved is an active edge which is intersected with the circle. The active edge intersected with the circle is (b, c) as illustrated in Fig. 12a. The intersection point of the circum circle with (b, c) has been marked as point y. Based on

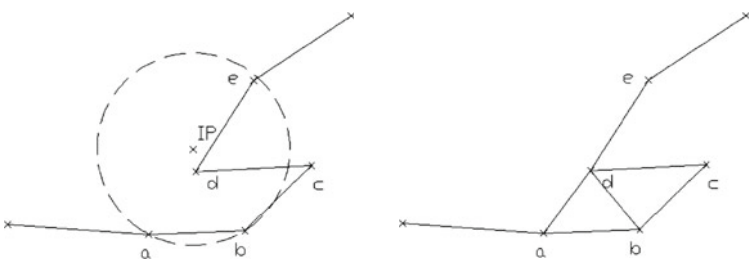

Fig. 11 **a** Two types of object lie within the *circle* which are active nodes and active edges. **b** A *triangular element* is constructed

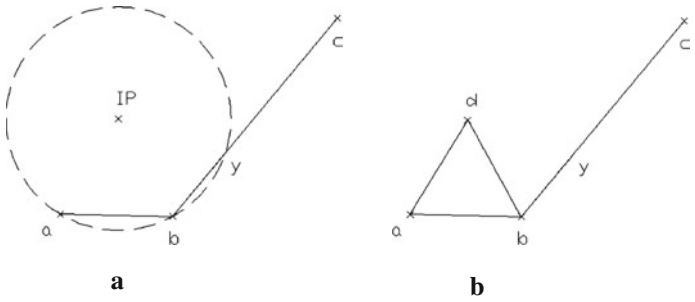

a b

Fig. 12 **a** An active edge intersected with the *circle*. **b** The IP becomes node *d*, the new active node for *triangular element*

a b

Fig. 13 **a** The intersected active edge is (b, c). The length of intersection point *y* and the node *b* of base edge is more than the length of the radius. **b** The triangular element is constructed by connecting the node associated with the intersected active edge to the base edge

the algorithm of XAFT, the length between the intersection point and the connected node of the base edge needs to be determined. In order words, referring to Fig. 12a, the length between node *b* and point *y* needs to be determined. If the length is less than the radius of the circle; therefore, the intersected active edge is disregarded and the IP becomes the third vertex of the triangular element. Based on Fig. 12b, the IP becomes node *d* in which a triangle element is constructed with edges (a, b) (a, d) and (b, d) as the three sides of the triangular element.

Case 5 Slightly different from Case 4, if the length between the intersection point *y* and the connected node of the base edge is more than the length of the radius of the circle; therefore, the active edge intersected with the circle is considered in which the node of the active edge is selected as the third vertex. In other words, referring to Fig. 13a, since the length of point *y* and node *b* is more than the length of the radius; therefore, node *c* which is the node associated with active edge (b, c) is selected to be the vertex to form triangle elements as illustrated in Fig. 13b. This condition belongs to Case 5.

However, if there are multiple edges intersecting with the circle and they are all satisfying the condition of Case 5; therefore, the associated node which is the closest to IP is selected as the third vertex.

Case 6 For the last case in XAFT (Case 6), let us say the base edge considered is (a, b)as illustrated in Fig. 14a. The only object that can be found in the constructed circle is an active edge with the condition of every edge being equal to the length of the radius and the nodes associated with the active edges must be at the circum circle. Let us say the number of the active edges satisfying the condition of Case 6 is N; therefore, $N + 1$ number of triangular elements are constructed. This is achieved when all the nodes at the circum circle are connected to the IP, hence the IP is selected as the vertex for all triangular elements. All the elements are equilateral triangles since the sides or edges are all equal. This can be referred in Fig. 14a where there a re two active edges intersecting with the circle which are (b, c) and (d, e). At the same time these edges have an equal length to the radius of the circle as well as all nodes associated with these edges being at the circum circle, namely nodes b, c, d and e. Therefore, three equilateral triangle elements are constructed as illustrated in Fig. 14b.

It must be noted that Case numbers 3, 4, 5 and 6 which are incorporated in the algorithm of XAFT are able to solve the problem highlighted by [10] specifically in the third point whereby considering these six categories of cases, triangular elements can be constructed directly in every iteration without having to erase a few existing elements or to re-order the Front.

XAFT for domains with one inner boundary is summarized as follows:

Step 1: Generate nodes at the outer boundary and inner boundary of the computational domain. Apply the layer concept at the desired location along the boundary. From the nodes at the boundary, boundary edges will be formed. The set of all boundary edges (both at outer and inner boundary) will now be the initial Front.

Step 2: Start to generate triangular elements at inner boundary edges of the Front list.

Step 3: Select the active edge with the shortest length in the Front list. The current selected edge being considered is called the base edge.

Step 4: Compute the ideal point (IP) on the perpendicular bisector of the base edge in such a way that an equilateral triangle is formed with the IP as the vertex.

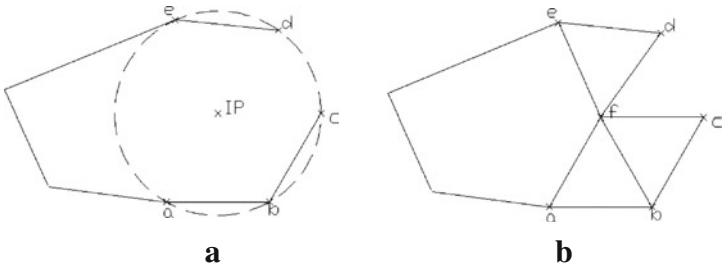

Fig. 14 **a** Two active edges with equal length to the radius intersected with the *circle* and at the same time all the nodes of the active edges are at the circum circle. **b** *Three equilateral triangle elements* are constructed simultaneously

Step 5: Construct a circle with a radius equal to the length of the base edge. Determine any objects such as active nodes lying within the circle or intersected active edges with the circum circle.

Step 6: Generate the triangular element based on the six categories of cases below:

Case 1 No active nodes lie within the circle. IP is selected as the vertex. Equilateral triangle will be formed.

Case 2 Active nodes lie within the circle. Compute the distance of all the active nodes and the IP. The closest point to the IP will be selected as the vertex.

Case 3 Three active edges are connected to themselves. Therefore, the three edges will automatically form triangular elements.

Case 4 No active node lies within the circle. However, there is an active edge intersecting with the circle, but the length of intersection points with the node of the base edge is less than the length of the radius of the circle. Therefore, the intersected active edge is disregarded and instead the IP will become the vertex.

Case 5 No active node lies within the circle. However, there is an active edge intersecting with the circle and the length of intersection points with the node of the base edge is equal or more than the length of radius. Therefore, the nodes associated with the intersected edge will be considered in which the node that is closer to the IP will be selected as the vertex to form a new element.

Case 6 The length of N intersected active edge is equal to the length of the radius and all the nodes associated with the intersected active edges are at the circum circle. Therefore, a number of $(N+1)$ equilateral triangles will be formed with IP as a vertex.

Step 7: Update the Front by deleting the base edge. The new active edges created during the triangulation element will be added to the Front list.

Step 8: Repeat Steps 2–7 until there is no active edge at the inner boundary left.

Step 9: Repeat Steps 3–7 until all the remaining parts of the domain have been covered or have been triangulated.

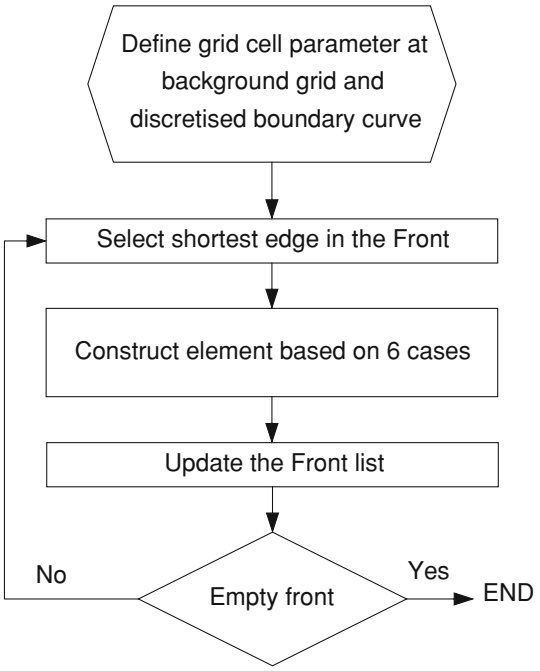

Fig. 15 The general scheme of XAFT

The general scheme of XAFT is illustrated in Fig. 15 where it can be seen that the element construction procedure is based on six cases of consideration, instead of only two in SAFT as illustrated in Fig. 6.

4.1 The Layer and Depth Concept

XAFT makes use of the layer concept at the appropriate boundary curve or line. The aim of employing the layer/depth concept is to divide a line into several segments with different lengths linearly. The length Ld_i of layer d_i with $i = 1, 2, \ldots, m$ is given as

$$Ld_i = i \frac{L}{\sum_{k=1}^{m} k}. \tag{21}$$

In the above equation, L is the total length of the straight line while m is the number of layers needed.

The line or boundary curve that is divided using the layer concept produces several smaller line segments with different lengths linearly. A set of nodes is placed at the end of each

a **b**

Fig. 16 **a** A straight line *AB* before applying the layer concept. **b** A set of nodes are placed at the line segments produced by employing the layer concept at line *AB*

Table 1 The result for layer concept for Fig. 16b

Layer, d_i	Length of layer, Ld_i	Layer d_i	Length of layer, Ld_i
d_1	$Ld_1 = (1)\frac{1.34}{1+2+3+4+5+6} = 0.0638$	d_4	$Ld_4 = (4)\frac{1.34}{1+2+3+4+5+6} = 0.2552$
d_2	$Ld_2 = (2)\frac{1.34}{1+2+3+4+5+6} = 0.1276$	d_5	$Ld_5 = (5)\frac{1.34}{1+2+3+4+5+6} = 0.3190$
d_3	$Ld_3 = (3)\frac{1.34}{1+2+3+4+5+6} = 0.1914$	d_6	$Ld_6 = (6)\frac{1.34}{1+2+3+4+5+6} = 0.3830$

newly divided segment line. Figure 16a illustrates a straight line before applying the layer concept while Fig. 16b illustrates m number of smaller segment lines or edges resulting from the layer concept applied at AB. For illustration, let say the length of the straight line AB as in Fig. 16a is $L = 1.34$ and the number of layer required is $m = 6$. The following Table 1 shows the layer and its length for every layer.

Referring to Fig. 1b, only the left wall and the bottom wall is divided into active edges based on the predetermined placement of sensor deployments represented as nodes. However, no nodes existed along the upper and right outer boundary since only one quarter of the simplified furnace is considered in this study. Therefore, the layer concept is proposed to be used at the upper and right outer boundary in order to generate the nodes and edges along the boundary. Referring to Fig. 8b, nodes 1, 2 and 3 at the right outer boundary and nodes 9 and 10 at the upper outer boundary are the nodes generated by applying the layer concept.

4.2 Significance of XAFT

The significance of the XAFT is as follows:

1. No grid cell parameters for all elements are required in XAFT, instead, only the number of reading points at specific boundaries or areas needs to be determined. The size of the triangular elements generated in the whole domain is controlled by the layer concept applied at the desired boundary as well as the boundary edges from the pre-determined location of the sensors.
2. No empirical rule of Eq. (1) is needed to calculate the radius of the circle as in SAFT. In order to construct the circle for the six cases under consideration, the radius is set to be equal to the length of the base edge considered. Consequently, the part of calculating the radius in the algorithm of EAFT is simpler compared to the SAFT with the empirical rule.
3. Six categories of cases or conditions are identified in order to determine how to generate the triangular element directly using XAFT. This is an extension of the existing cases of the SAFT. As a matter of fact, the six categories of cases are able to solve the problem of erasing a few existing elements, or the need to re-order the Front when there is an undecided element creation in the iteration.
4. A stitching method of connecting the boundary triangular element with the inner triangular element is automatically provided within the same algorithm in XAFT. It is guaranteed to connect the boundary element and the ideal triangulation element (equilateral triangle) in the computational domain. Hence, no additional temporary layer of near boundary elements needs to be generated as proposed in [8] for the stitching method.

4.3 XAFT Illustration in Element Construction Using a Simple Case

We illustrate XAFT through a simplified case as our initial study. Figure 1b shows the horizontal cross-section of one quarter of the whole furnace showing a single heating coil and a set of four sensor nodes distributed along the inner wall of the furnace. Using Fig. 1b as our foundation for the conceptual model, a set of nodes is placed along the outer boundary curve (the inner furnace wall) and along the inner boundary curve (the coil) as illustrated in Fig. 17.

Example 1 IP is computed and becomes the centre of the circle constructed with a radius equal to the length of the base edge as illustrated in Fig. 18a. Since there is no active node lying within the circle and none of active edges in the Front intersect with the circle, therefore, the IP becomes the vertex for the first triangular element. An equilateral triangle is constructed as illustrated in Fig. 18b. This belongs to Case 1 in the XAFT. The first triangular element for the domain is $e\,[1] = [17, 18, 25]$. In other words, the triangular element is a combination of edge (17, 18), (18, 25) and (25, 17) as the three sides of the triangle. Node 25 is the new node generated in the domain which replaces IP as a vertex for the new triangular element.

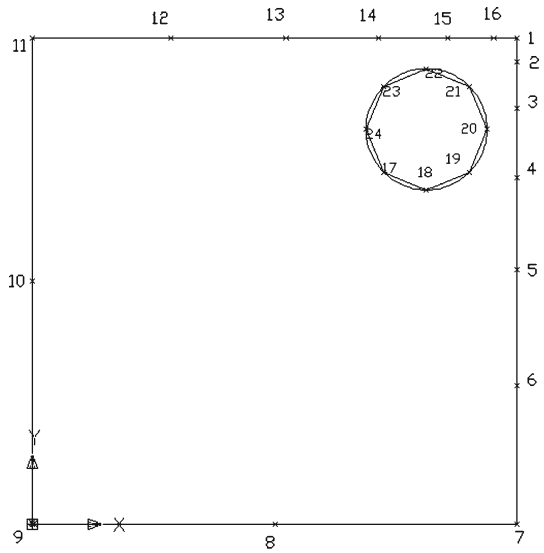

Fig. 17 Initial nodes are placed along the *outer boundary* and *inner boundary* before the unstructured triangular grids are generated

Example 2 A circle with its centre at IP is constructed as in Fig. 19a. Node 4 which is an active node lies within the circle. This condition belongs to Case 2, therefore node 4 is selected as a vertex of the third triangular element. The new element is $e\,[3] = [19, 20, 4]$.

Example 3 Steps 3–7 as in the algorithm proceed until all the inner boundary edges become passive edges and are deleted from the Front list as illustrated in Fig. 20a. At the same time, two triangular elements are constructed automatically since the three active edges are connected among themselves. This condition belongs to Case 3 as illustrated in Fig. 20b. The new triangular elements are $e\,[9] = [3, 4, 20]$ and $e\,[10] = [14, 15, 22]$. It must be noted that the Front needs to be updated every time a new triangular element is constructed.

Example 4 The base edge considered is $(27, 28)$ as illustrated in Fig. 21a. No active node lies within the circle. Active edge $(13, 27)$ intersects with the circle, but the distance of intersection points at the edge with node 27 is less than the length of the radius. This condition belongs to Case 4. Therefore, $(13, 27)$ is not considered to be the side for the new triangular element. Instead, the IP is selected to be the vertex of the triangular element where it becomes node 29. The new triangular element generated is of type equilateral triangle which is $e\,[22] = [27, 28, 29]$ as illustrated in Fig. 21b.

Example 5 The base edge considered is $(33, 31)$as illustrated in Fig. 22a. Edge $(12, 31)$ intersects with the circle and the distance of the intersection point at edge $(12, 31)$ with node 31 of the base edge is more than the length of the radius. Therefore, the node associated with the intersected edge is considered as explained in Case 5. In this particular condition, node 12 is associated with $(12, 31)$. Since node 12 is the only node to be considered; therefore, node 12 is selected to be the vertex of the new triangular element as can be seen in Fig. 22b. The new element is $e\,[31] = [33, 31, 12]$.

Example 6 The base edge considered is $(35, 40)$ as illustrated in Fig. 23a. Two active edges intersected with the circle and both lengths of the active edges are equal to the length of the radius as well as the nodes associated with the active edges lie at the circum circle. Therefore, three equilateral triangles are constructed with the IP selected as the vertex and become node 41 as can be seen in Fig. 23b. This condition belongs to Case 6. The new triangular elements constructed are $e\,[49] = [35, 40, 41]$, $e\,[50] = [32, 35, 41]$ and $e\,[51] = [30, 32, 41]$.

4.4 Integration of the Unstructured Grid with the Governing Equation of Radiative Heat Transfer

The sensors placed along the wall in this conceptual model can assist in calculating the initial intensity at the boundary of the enclosure using the equations in Sect. 3.2. It must be noted that in order to have initial intensity values at the boundary, the function of the sensors is to collect the value of temperature at the wall. Let us say nodes N_i $(i = 1, 2, \ldots, n)$ are the outer boundary nodes and at the same time, all of these nodes represent the predetermined location of the sensors. The boundary edge is formed by connecting these sensors at the enclosure, and these sensor boundary edges are denoted as $Edge\_sensor_i = (N_i, N_{i+1})$.

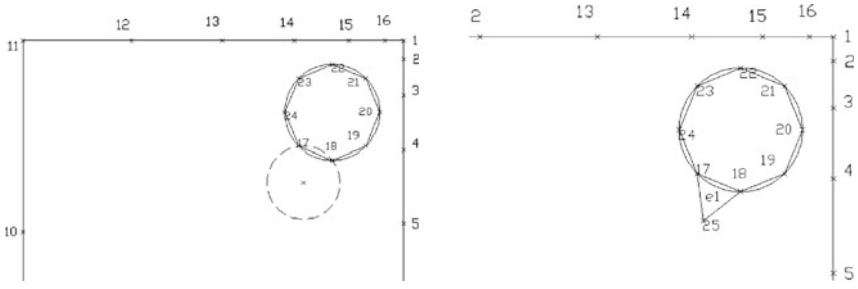

a **b**

Fig. 18 **a** A *circle* with radius equal to the length of base edge and with centre at IP is constructed. **b** *Equilateral triangle* is formed since no node lies within the circle following case 1

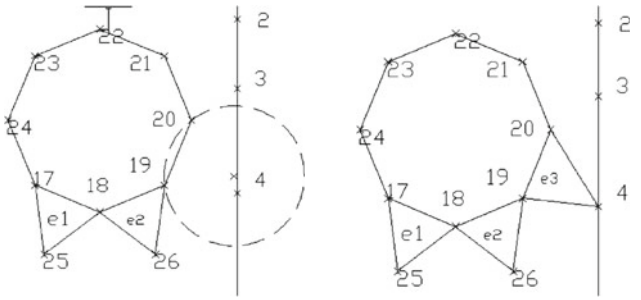

Fig. 19 **a** *Circle* with radius equal to the length of base edge and centre at IP is constructed **b**. Node 4 is selected as a vertex to form a triangular element following case 2

As a matter of fact, these sensor boundary edges are among the edges forming a triangular element. Let us say the temperature obtained from the sensors at the outer boundary node N_i are denoted by T_i. The average temperature value of $Edge\_sensor_i = (N_i, N_{i+1})$ at the boundary or at the enclosure will be:

$$\text{TEdge\_sensor}_i = \frac{T_i + T_{i+1}}{2} \tag{22}$$

Once the value of TEdge_sensor_i is obtained, the value will be replaced in the T of Eq. (3) in order to get the value of blackbody intensity. Therefore, Eq. (3) can be rewritten as

$$I_\text{b} = E_\text{b}/\pi = \sigma(\text{TEdge\_sensor}_i)^4/\pi \tag{23}$$

The intensity of blackbody obtained from the above equation is substituted in the boundary condition in Eqs. (7) and 10), since the boundary face is a part of the enclosure surface. The calculation is done element by element until all directions have been covered and the convergence criteria are met.

4.5 The Advantages of XAFT

The whole process of the fluid flow simulation in computational fluid dynamics (CFD) involves all three elements namely pre-processing, solving and the post-processing. As a matter of fact, the XAFT which is a newly developed unstructured triangular mesh generation algorithm, falls into the pre-processing element in CFD. The advantages of XAFT are as follows

1. The algorithm of XAFT is simpler where it does not need both grid cell parameter and empirical rule for all elements as in SAFT.
2. The six categories of cases for element creation procedure are able to cover all kinds of condition during element creation in mesh generation hence the problem of sudden undecided element creation is solved.
3. The XAFT provides framework for case-study involving sensors deployment for boundary value problem. To date, no mesh generation algorithm that distinguish the existence of sensors at the boundary. On the other hand,

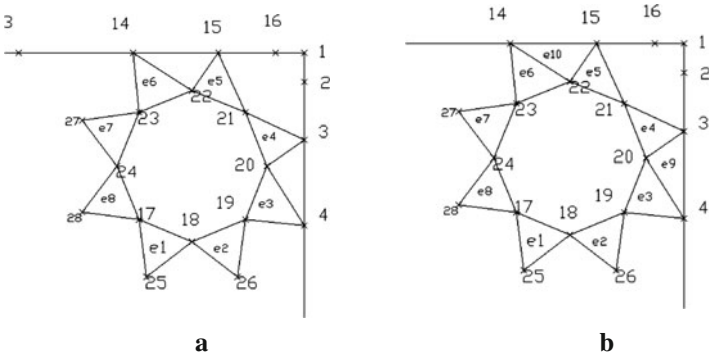

Fig. 20 **a** All the inner boundary edges are completely triangulated. **b** *Two triangular elements* are constructed automatically following case 3

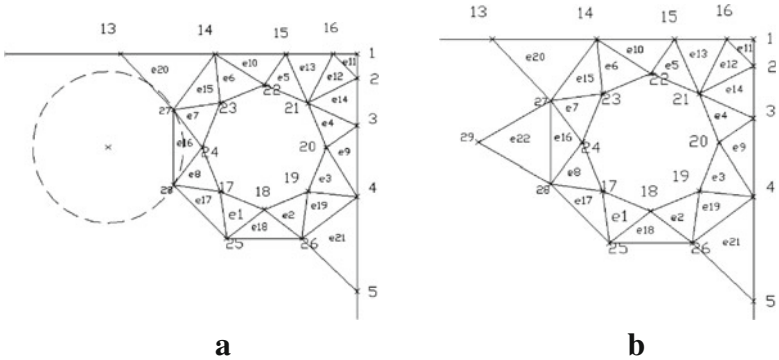

Fig. 21 **a** The length of the intersected point of active edge with the node of the base edge is less than the radius of the *circle*. **b** *Equilateral triangle* is formed since it belongs to case 4

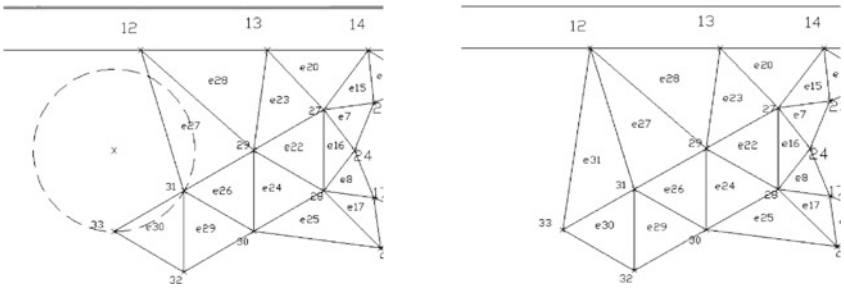

Fig. 22 **a** The length of the intersection is more than the radius of the *circle*. **b** New element constructed by selecting the intersected edges with the *circle* as new side to form element following case 5

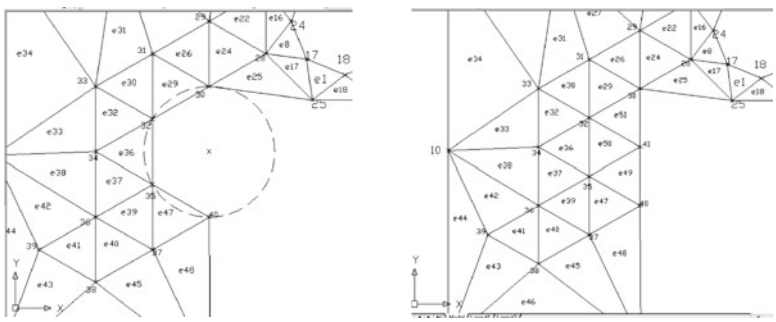

Fig. 23 **a** Two active edges intersect the *circle* with both lengths equal to the radius and the nodes of the active edges are exactly at the *circum circle*. **b** *Three equilateral triangles* are constructed following case 6

the XAFT acknowledge the existence of the sensors and ensure the location of the sensor as boundary nodes in computational domain. Therefore, different values of specific variables such as temperature can be obtained according to the location of the sensors deployment. Hence, different values of the boundary face can be assigned easily along boundary layers in the CFD software code such as FLUENT when the resulted mesh is integrated with governing equations.

5 The Difference Between SAFT and XAFT

Both SAFT and XAFT set up a group of oriented line segments connecting nodes on the boundary as an initial Front. A background grid composed of a minimum number of elements is generated in SAFT and all the nodes of this element are specified with the grid cell parameters (size δ, stretching s and orientation of the cells ϕ). Then, the grid cell parameters for all nodes in the Front are interpolated when constructing the triangular element in the domain in SAFT. On the other hand, no parameters are needed for XAFT where the user only needs to specify how many sensors are needed together with their location to be employed, the number of reading points at the inner boundary as well as generating nodes using the layer concept at the appropriate boundary.

In SAFT, the active edge in the Front with the shortest length is selected and it does not matter if it starts with inner boundary edges or outer boundary edges. However, priority is given to inner boundary edges in XAFT, where the shortest length of edges is selected. It must be noted that the XAFT requires that all the inner boundary edges become passive in the Front which means that the entire inner boundary edge had been completely triangulated then continues with the rest of other active edges in the Front.

SAFT requires the empirical rule as in Eq. (1) to obtain the radius of the circle for the element creation procedure while XAFT uses a simpler method where the radius is set to be equal of the base edge. Besides that, in order to determine the construction of equilateral triangles in SAFT, the only condition that needs to be satisfied is that there are no such active nodes lying within the circle. However, the condition for XAFT is stricter in which no objects such as active nodes as well as intersected active edges are allowed to lie within the circles when constructing equilateral triangle. An exception is given for only case 6 in XAFT. In general, the XAFT has come out with a set of six structured categories of cases when constructing the triangular element, unlike SAFT.

6 Experimental and Simulation Results

A simulation of one quarter of the furnace as a simplified version of the initial conceptual model was performed using FLUENT where sensors were assumed to be placed at the inner furnace wall as illustrated in Fig. 1b. Only the left and bottom boundary curves of the conceptual model have the sensors deployed, where these particular boundary curves are

Table 2 The results for the layer concept applied to Fig. 17

Layer, d_i	Length of layer, Ld_i	Layer, d_i	Length of layer, Ld_i
d_1	$Ld_1 = (1)\frac{8}{\sum_{k=1}^{6} k} = 0.3809$	d_4	$Ld_4 = (4)\frac{8}{\sum_{k=1}^{6} k} = 1.5238$
d_2	$Ld_2 = (2)\frac{8}{\sum_{k=1}^{6} k} = 0.7619$	d_5	$Ld_5 = (5)\frac{8}{\sum_{k=1}^{6} k} = 1.9048$
d_3	$Ld_3 = (3)\frac{8}{\sum_{k=1}^{6} k} = 1.1429$	d_6	$Ld_6 = (6)\frac{8}{\sum_{k=1}^{6} k} = 2.2857$

automatically discretized according to the location of sensor deployments. However, since the upper and right boundary curve is not a real boundary wall and does not have sensors deployed there; therefore, a set of nodes are generated along these boundaries by using the layer concept to produce edges with different length linearly. The lengths of the layers obtained are shown in Table 2 where the number of layer is 6 with an overall length of 8.

Layers d_1, d_2, d_3, d_4, d_5 and d_6 are applied at the top boundary curve and represented by edges (16, 1), (15, 16), (14, 15), (13, 14), (12, 13) and (11, 12), respectively, as can be seen in Fig. 17. The same procedure is applied at the right boundary curve of the domain. Layers d_1, d_2, d_3, d_4, d_5 and d_6 are applied to the right hand side of the boundary domain and represented by edge (1, 2), (2, 3), (3, 4), (4, 5), (5, 6) and (6, 7), respectively. Therefore, nodes 1–6 and nodes 12–16 are points resulted from layer concept applied. Nodes 7–11 denote the sensors location. On the other hand, nodes 17–24 are the reading points needed in the study.

At the end of the process, the mesh obtained using XAFT is illustrated in Fig. 24. Starting from the initial Front with 24 nodes, the final mesh with 42 nodes and 60 triangular elements covering the computational domain is obtained. Every node that is generated is numbered as well as the resulting triangular element. The element is numbered followed by the notation 'e'. It can be seen that the first eight elements are generated along the inner boundary edges at the circum circle and then followed by the shortest edges in the updated Front list and finally covering the whole computational domain.

All triangular elements covering the computational domain are definitely not of equal size since in this specific problem, it is required that the location of the sensors itself are regarded as the nodes forming the boundary element. The ratio between the shortest and the longest edge is 1:11.84 showing the degree of the non-uniform edge nodes distribution. However, a number of equilateral triangles are formed where appropriate such as at the centre of the domain as well as at some part of the inner boundary edges at circum circle. It is also proven that XAFT is able to stitch the boundary element with the ideal mesh of equilateral triangle in the domain within the same algorithm.

In order to examine the quality of the initial unstructured mesh, an EquiAngle Skew Q_{EAS}, which is a normalized measure of skewness is used which is defined as follows [20]

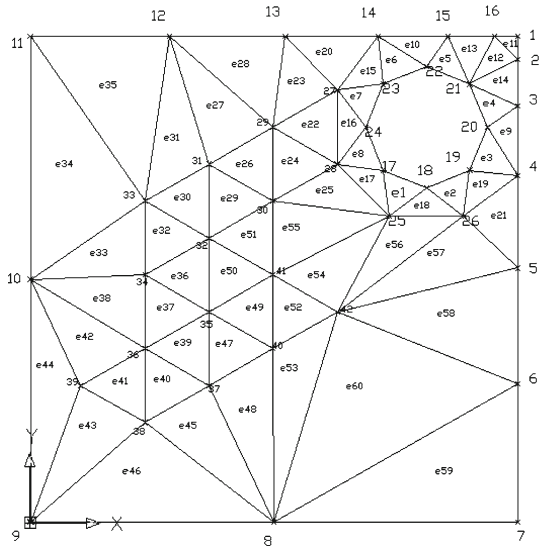

Fig. 24 Unstructured mesh produced by XAFT

$$Q_{\mathrm{EAS}} = \max\left\{\frac{\theta_{\max} - \theta_{\mathrm{eq}}}{180 - \theta_{\mathrm{eq}}}, \frac{\theta_{\mathrm{eq}} - \theta_{\min}}{\theta_{\mathrm{eq}}}\right\} \tag{24}$$

In the above equation, $\theta_{\max}$ and $\theta_{\min}$ are the maximum and minimum angles (in degrees) between the edges of the triangular element and θ_{eq} is the characteristic angle corresponding to an equilateral element of triangular where in this particular case, $\theta_{\mathrm{eq}} = 60°$. The value of the examined quality based on this equation provided by [20] is in the range of $0 \leq Q_{\mathrm{EAS}} \leq 1$ where $Q_{\mathrm{EAS}} = 0$ if the element is equilateral triangle and $Q_{\mathrm{EAS}} = 1$if the triangular element is degenerate (poorly shaped). Figure 25a–d illustrate the corresponding triangular element in the mesh with respect to the range of the quality examined.

Of all the triangular elements generated, 33.33 % are equilateral triangles and only 15 % fall into average or fair quality range $0.5 < Q_{\mathrm{EAS}} \leq 0.75$ where the highest value for the element quality is $Q_{\mathrm{EAS}} = 0.717$.The overall relationship between $Q_{\mathrm{EAS}}$and element quality is illustrated in Table 3 [20]. The total number of elements with respect to the range of element quality can be referred to the same table. Therefore, the initial triangular elements generated using the XAFT are all valid and independent of its size as well as none of it is degenerate or poorly shape. Mesh post-processing is not required in this case since the quality of the initial mesh is good and acceptable for further simulation.

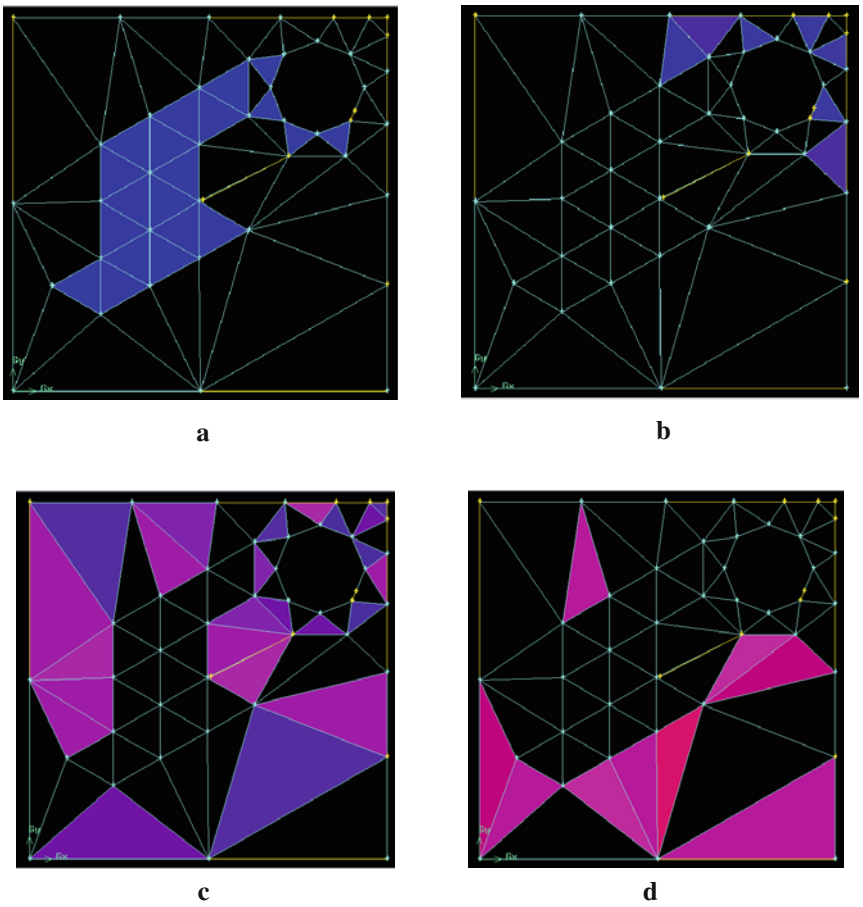

Fig. 25 **a** Element with quality $Q_{EAS} = 0$. **b** Element with quality $0 < Q_{EAS} \leq 0.25$. **c** Element with quality $0.25 < Q_{EAS} \leq 0.5$. **d** Element with quality $0.5 < Q_{EAS} \leq 0.75$

Table 3 The relationship between Q_{EAS} and mesh quality together with the total element in the range, respectively

Q_{EAS}	Mesh quality	Total element in percentage
$Q_{EAS} = 0$	Equilateral (perfect)	33.33
$0 < Q_{EAS} \leq 0.25$	Excellent	11.67
$0.25 < Q_{EAS} \leq 0.5$	Good	40
$0.5 < Q_{EAS} \leq 0.75$	Fair	15
$0.75 < Q_{EAS} \leq 0.9$	Poor	0
$0.9 < Q_{EAS} \leq 1$	Very poor (sliver)	0
$Q_{EAS} = 1$	Degenerate	0

In order to prove that the triangular mesh works well and is appropriate for computational analysis, the governing equation of radiative heat transfer is incorporated with the mesh. Using FLUENT version 6.0, simulation is conducted to solve the radiative heat transfer by using the discrete ordinate methods. Since this is a conceptual model, the value of the wall temperature at every sensor is imposed so that the temperature value is used as boundary values in the calculation.

Figures 26 and 27 show the flue gas temperature distribution contours and incident radiation between the walls, respectively. As shown in the simulation results, the temperature distribution of the flue gas is non-uniform, which will further influence the heat transfer between the wall and the reactor tube/coil. The temperature at the reactor tube/coil is affected by the flue gas distribution since flue gas transfers the heat to the reactor/coil. The highest temperature value at the coil is 1,479.71 K and the lowest is 1,241.674 K, meaning the difference is as high as 238.036 K. The location of highest temperature value occurs in the simulation resulted in having highest incident radiation values when both Figs. 26 and 27 are compared together. The simulation is conducted until convergence is reached at iteration 104 as illustrated in Fig. 28. However, it must be noted that the value used in the simulation is just an imposed value. The main interest is to prove that the unstructured mesh generated using the algorithm of XAFT is appropriate for further analysis such

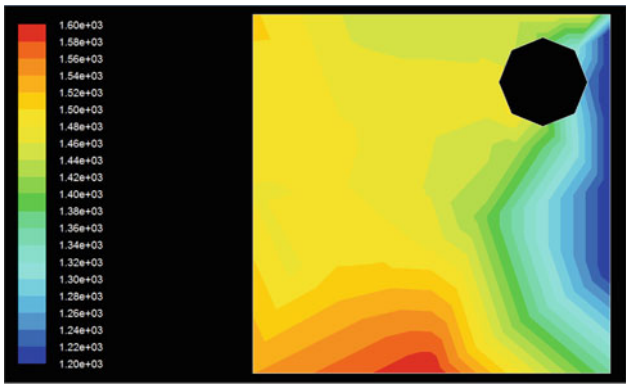

Fig. 26 The contour of temperature distribution of the flue gas

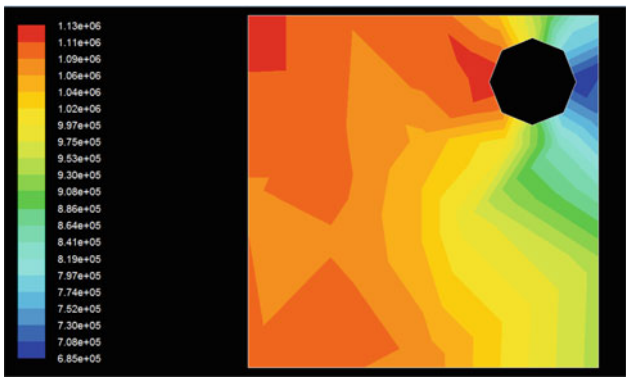

Fig. 27 The contours of incident radiation

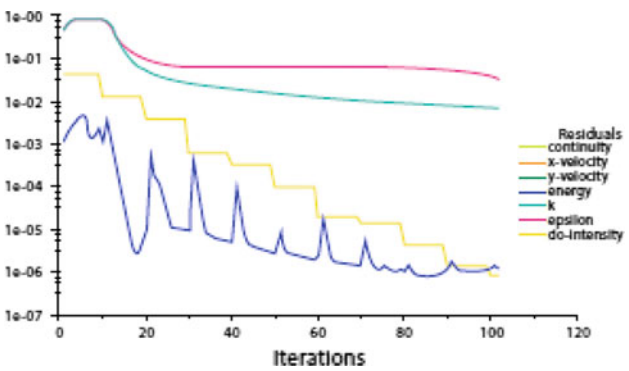

Fig. 28 Scaled residuals for the iterations

as to analyze radiative heat transfer when combining with the value read by the sensors as boundary value.

7 Summary and Conclusion

A new technique called XAFT has been proposed, and this technique is proven to be effective in generating initial unstructured grids/meshes for modeling radiative heat transfer in ethylene cracker furnaces. XAFT incorporates the layer concept to generate nodes which form edges in varying lengths linearly at appropriate boundary curves as well as introduced the structured six cases of consideration for the element creation procedure. The differences between XAFT and the SAFT are outlined in the paper. The triangular mesh forms the domain for approximating the radiative heat transfer using the discrete ordinate method. Simulations using FLUENT are performed on the triangular mesh to obtain the numerical approximations. The results obtained support the findings in XAFT for effectively approximating the radiation intensity and temperature values inside the furnace.

References

1. Gielen, D.; Bennaceur, K.; Tam, C.: IEA petrochemical scenarios for 2030–2050: Energy technology perspectives. http://www.iea.org/textbase/work/2006/petrochemicals/Discussion_Paper.pdf (2006). Accessed 17 Dec 2008
2. Heynderickx, G.J.; Nozawa, M.: High-emissivity coatings on reactor tubes and furnace walls in steam cracking furnaces. Chem. Eng. Sci. pp. 5567–5662 (2004)
3. Modest, M.F.: Radiative Heat Transfer, 2nd edn. Academic Press, New York, p. 822 (2003)
4. Lohner, R.: Progress in grid generation via the advancing front technique. Eng. Comput. pp. 186–210 (1996)
5. Farrashkhalvat, M.; Miles, J.P.: Basic Structured Grid Generation With An Introduction To Unstructured Grid Generation. Butterworth-Heinemann, Oxford (2003)
6. Naji, H.S.: An improved advancing front algorithm for triangulating arbitrary two dimensional regions (2004)
7. Minyi, K.; Jie, C.; Huazhong, J.: Research of using dynamic programming in the nodes encoding optimization. In: International Conference on Information Engineering and Computer Science (2009)
8. Sazonov, I.; et al.: A stitching method for the generation of unstructured meshes for use with co-volume solution techniques. Comput. Methods Appl. Mech. Eng. **195**, 1826–1845 (2006)
9. Ito, Y.; et al.: Parallel unstructured mesh generation by an advancing front method. Math. Comput. Simul. **75**, 200–209 (2007)
10. Kovac, N.; Gotovac, S.; Poljak, D.: A new front updating solution applied to some engineering problems. Arch. Comput. Methods Eng. **9**, 43–75 (2002)
11. Persson, P.O.: Lecture 1 Computational Mesh Generation. MIT (2008)
12. Zhu, J.; Blacker, T.; Smith, R.: Background overlay grid size functions. In: Proceedings of the 11th International Meshing Roundtable, pp. 65–74 (2002)
13. Lyra, P.R.M.; Carvalho, D.K.: A computational methodology for automatic two-dimensional anisotropic mesh generation and adaptation. J. Braz. Soc. Mech. Sci. Eng. **28**(4), 399–412 (2006)
14. Seveno, E.: Towards an adaptive advancing front method. In: 6th International Meshing Roundtable (1997)
15. Peraire, J.; Peiro, J.; Morgan, K.: Advancing front grid generation. In: Weatherill, N.P.; Soni, B.K.; Thompson, J.F. (eds.): Handbook of Grid Generation. CRC Press LLC, Boca Raton (1999)
16. Blazek, J.: Principles of grid generation. In: Computational Fluid Dynamics: Principles and Applications (2007)
17. Versteeg, H.K.; Malalasekera, W.: An Introduction to Computational Fluid Dynamics. Pearson Education, England (2007)
18. Stefanidis, G.; et al.: Gray/nongray gas radiation modeling in steam cracker CFD calculations. AIChE J. **53**(7), 1658–1669 (2007)

19. Lan, X.; et al.: Numerical simulation of transfer and reaction processes in ethylene furnaces. Chem. Eng. Res. Des. **85**(A12), 1565–1579 (2007)

20. Gambit 2.3 Documentation—Gambit User Guide. http://my.fit.edu/itresources/manuals/gambit2.3/help/index.htm. Accessed 25 November 2010